Ultrasonics 131 (2023) 106953

Contents lists available at ScienceDirect

Ultrasonics

journal homepage: www.elsevier.com/locate/ultras

Increasing frame rate of echocardiography based on a novel 2D spatio-temporal meshless interpolation

Hamed Jalilian [a,1], Sajjad Afrakhteh [b,*,1], Giovanni Iacca [b], Libertario Demi [b]

[a] Department of Mathematics, Iran University of Science and Technology, Narmak, Tehran, Iran
[b] Department of Information Engineering and Computer Science, University of Trento, Italy

ARTICLE INFO

Keywords:
Echocardiography
Temporal super-resolution
Interpolation
Radial basis functions
Intensity variation time surface

ABSTRACT

Background: Increasing temporal resolution through numerical methods aids clinicians to evaluate fast moving structures of the heart with more confidence.

Methodology: In this study, a spatio-temporal numerical method is proposed to increase the frame rate based on two-dimensional (2D) interpolation. More specifically, we propose a novel intensity variation time surface (IVTS) strategy to incorporate both temporal and spatial information in the reconstruction. In this regard, we exploit radial basis functions (RBFs) for 2D interpolation. The reason for choosing RBFs for this task is manifold. First, RBFs are able to interpolate on large-scale datasets. Moreover, their mathematical implementation is simple. Another important property of this interpolation technique, which is addressed in this study, is its meshless nature. The meshless property enables higher up-sampling (UpS) rates for echocardiography to improve temporal resolution without noticeably degrading image quality. To evaluate the proposed approach, we tested the RBF interpolation on 2D/3D echocardiography datasets. The reconstructed frames were analyzed using different image quality metrics, and the results were compared with two popular techniques from the literature.

Results: The findings demonstrated that, with a down-sampling rate of 3, the proposed technique outperformed the best existing method by 42%, 87%, 8%, and 11%, respectively, in terms of mean square error (MSE), contrast to noise ratio (CNR), peak signal-to-noise ratio (PSNR), and figure of merit (FOM). It should be noted that the proposed method is comparable to the best available method in terms of structural similarity (SSIM) index. Furthermore, when compared to the original images, the results of employing our technique on radio-frequency (RF) level analysis demonstrated that the reconstruction accuracy is satisfactory in terms of image quality criterion.

Conclusion: Finally, it is worthwhile noting that the proposed method is better than (or comparable to) the other methods in terms of reconstruction performance and processing time. Therefore, the RBF interpolation can be a promising alternative to the existing methods.

1. Introduction

Medical ultrasound imaging is one of the most important techniques for diagnostics which is used to monitor the internal body motions. Images provided by this tool are based on radiation and reflection of sound waves with a frequency higher than 20 kHz. The backscattered signals returned from the body are processed and then the ultrasound image is beamformed. One of the advantages of this method is its non-invasive property, compared to CT scans, as the patient is not exposed to radiation. After processing the signals reflected from the body, several methods can be used to reconstruct the information obtained from the backscattered ultrasound wave fields (from fundamental or harmonic components) in the form of images, such as A-mode, B-mode, and Doppler [1].

Temporal resolution is a crucial aspect in ultrasound imaging. It is typically expressed in terms of frame rate, i.e., the number of frames displayed per second. Temporal super-resolution (i.e., increasing frame rate) is necessary in many diagnostic tasks. In echocardiography, it helps physicians assess faster heart movements, especially in the valves. Current echocardiography systems provide frame rates and volume rates of 30 to 80 frames per second and 10 to 20 volumes per second, respectively for two-dimensional (2D) and three-dimensional (3D) ultrasound imaging of a normal adult heart. Nevertheless, higher frame

* Corresponding author.
E-mail address: sajjad.afrakhteh@unitn.it (S. Afrakhteh).
[1] Equal contribution.

https://doi.org/10.1016/j.ultras.2023.106953
Received 25 November 2022; Received in revised form 3 February 2023; Accepted 9 February 2023
Available online 13 February 2023

rates are required to capture mechanical characteristics or transient events of the heart, particularly in 3D echocardiography [2,3].

Previous literature has presented various pre-processing methods for improving the frame rate, based on changing the configuration of the acquisition system used for the signal transmission and reception [4]. One of these solutions is multi-line acquisition (MLA) [5], which is employed in most of the currently available commercial systems. This technique is able to boost the frame rate without sacrificing line density or sector width. The method reconstructs many nearby lines simultaneously for each transmits beam. For example, a 4-MLA system beamforms four lines in parallel for each transmission beam, resulting in a 4-fold increase in frame rate. However, to make this possible, the transmit beam must be broadened, to guarantee that the area covered by a particular set of parallel receive lines is sufficiently insonified. This can be obtained by using a smaller aperture. However, it leads to less transmission energy and therefore reduced image quality (i.e., signal-to-noise ratio (SNR)). Another alternative is to employ the multi-line transmission (MLT) method, which entails transmitting pulses concurrently in various directions ultimately enabling the generation of multiple image lines in parallel [6–9]. In [10], discrete cosine transform (DCT)-based reconstruction was proposed to reduce the compromise between image quality and frame rate. This technique is based on sparse beamforming of scan lines of each image, followed by DCT reconstruction for improving the image quality. However, by using this method an information loss problem arises. Another approach for improving the temporal resolution is retrospective gating [11]. This method consists in dividing a large imaging sector into several smaller subsectors. Due to their small field of view (FoV), each of these subsectors is recorded across a single cardiac cycle at a high frame rate. Images from these subsectors are then merged using retrospective electrocardiogram (ECG) gating, to provide images of the whole imaging sector at the original temporal resolution. However, ECG gating may fail if the ECGs obtained during various cardiac cycles differ significantly. To address this issue, motion matching is an alternate approach for combining subsector images [12].

Another set of approaches, referred to as post-processing techniques, aims to enhance the temporal resolution of the beamformed images directly. Given that the method described in this article is a post-processing technique, we will introduce some representative works from the literature that aim to enhance temporal resolution during the post-processing stage. Perrin et al. [13] suggested the frame reordering approach for boosting temporal resolution in 3D echocardiography. Higher frame rates were accomplished by sampling over many beats and using a contemporaneous ECG signal to properly locate the frame inside the cardiac cycle. The manifold learning technique was used in [14] to extract nonlinear embedded information about echocardiography frames from successive frames in 2D manifold spaces. Each frame is projected as a point on the reconstructed manifold using this method. Hence, the connection between frames in the new domain may be derived based on the periodicity of the cardiac cycle. Then, a combination of this technique and cardiac cycles is used to increase the temporal resolution. Even though this technique can boost frame rate, it has a large computational complexity because of employing manifold learning strategy. Increasing the sample rate by using interpolation between sample frames has been proposed by Thaipanich et al. in [15]. This technique essentially slows down the ultrasound video, making it easier for physicians to detect and interpret any artifact. The authors have tested this method in two different situations. The first is when the video input changes abruptly, while the second is when the frame rate is low. Their proposed frame rate up conversion (FRUC) algorithm improved the peak signal-to-noise ratio (PSNR) by about 2.64 dB and 4.51 dB in the case of linear motion interpolation and frame repetition, respectively. In [16], a temporal alignment was created between 3D echocardiographic frames and magnetic resonance (MR) images using an adaptive non-rigid registration algorithm based on local phase mutual information on each temporally aligned image pair. Another similar method based on ECG signals has been proposed by Huang et al. in [17]. The authors have tried to produce equal number of frames compared to 3D echocardiography using the temporal interpolation of MR images. In [18], The intensity variation time curves (IVTCs) method was proposed to fit continuous curves to sample frames' pixels. Then, using Bayesian compressive sensing (BCS), sparse coefficients are found and approximated by IVTCs. Hosseinpour et al. [19] suggested a structure based on an acquisition scheme for temporal super-resolution based on compressive sensing (CS) theory. Their method was based on employing CS for the reconstruction of the IVTC of each pixel. By using this method, the frame rate increased by three times at the cost of high computational complexity arising from the CS post-processing. Yu et al. [20] developed a method for improving temporal resolution using deconvolution and spatio-temporal inter-frame correlation-based data collection. In another work, Mirarkolaei et al. [21] presented a motion-compensated interpolation algorithm for increasing the temporal resolution in echocardiography. To accomplish this, they specifically used a multi-scale bidirectional 3D speckle tracker in low frame rate acquisitions. Nevertheless, this method has limitations in selecting the proper kernel and search sizes. Khubani et al. [22] suggested a FRUC method based on Quaternion Wavelet Transform (QWT) to improve the motion estimation accuracy and reduce the computational complexity. Liu et al. [23] proposed a new strategy for super-resolution, in which a deep neural network learns the temporal dynamics of a video to calculate the ideal scale of temporal dependence adaptively. Then, to properly leverage the temporal link between successive low-resolution frames, they applied filters with various temporal scales to low-resolution input sequences, before adaptively aggregating them as in [24]. In [25], the authors proposed a novel frame rate up-conversion approach as a post-processing step during or after echo capture. The suggested approach uses both variational autoencoders (VAE) and generative adversarial networks (GAN) to generate realistic frames at a high frame rate that may be utilized to supplement traditional imaging. In [26] Jalali et al. proposed the cubic B-spline method to increase the temporal resolution of echocardiographic frames. They used a technique similar the IVTC introduced in [18], but based on B-spline method. In this method, the information between consecutive frames is approximated using B-spline interpolation. This method does not require motion estimation because it uses only pixels of the same position in the sample frames to reconstruct each pixel. This method can increase the frame rate up to two times without significant image quality degradation. We recently proposed a method designed to increase the frame rate of echocardiography by utilizing none-polynomial interpolation (NPI) [27,28]. The outcomes showed that, while the NPI technique does not increase computational complexity, it can be used to achieve better performance in terms of reconstruction error.

Interpolation methods are particularly beneficial since, in addition to maintaining the quality of the frames and increasing the temporal resolution, they are also characterized by good stability, high convergence and accuracy, and ease of implementation.

This study proposes a new technique for increasing the temporal resolution of echocardiography frames. The novelty of the presented study is to utilize a 2D interpolation method, which is called radial basis functions (RBFs), to increase the frame rate. Specifically, we proposed an intensity variation time surface (IVTS) approach to use the spatial and temporal information simultaneously throughout the entire video in the interpolation process. The procedure is carried out so that the IVTSs are first extracted based on the data gathered from the various rows of all the sample frames. The middle interpolated frames are then created by reconstructing the missing information of IVTSs using 2D interpolation. We compare the results of our proposed approach with those obtained by the methods proposed in [18,26], and show that the proposed method performs better not only in terms of quantity and quality, but also in terms of computational complexity.

The outline of the paper is as follows. In Section 2, the proposed method along with its material are described. We then describe the

Table 1
Examples of radial basis function basis.

Name	Abbreviation	Formula
Infinitely smooth:		
Multiquadric	MQ	$\phi(r)=\sqrt{1+(cr)^2}$
Inverse multiquadric	IMQ	$\phi(r)=\frac{1}{\sqrt{1+(cr)^2}}$
Gaussian	GA	$\phi(r)=e^{-cr^2}$
Piecewise smooth:		
Cubic	CU	$\phi(r)=\lvert r\rvert^3$
Thin plate spline	TPS	$\phi(r)=r^2Ln\lvert r\rvert$

suggested 2D RBF interpolator applied to image reconstruction. In Section 3, to demonstrate the effectiveness of the method, we apply our proposed technique to real echocardiographic data and comparisons are made with other approaches. Finally, in Section 4 we give the conclusions of this study.

2. Materials and methods

This section initially provides a brief explanation of the theory behind the proposed 2D interpolation based on RBFs, followed by the proposed procedure on how to use these functions to reconstruct echocardiography frames (i.e., increasing frame rate).

2.1. Radial basis functions theory

A well-established interpolation method is undoubtedly radial basic functions (RBFs). The 2D interpolation problem through RBFs can be presented as follows. Given the data $(X_j, y_j), j = 1,2,\dots,N, X_j \in \mathbb{R}^d, y_j \in \mathbb{R}$, the goal is to find a continuous function $S(X)$ so that $S(X_j) = y_j, j = 1,2,\dots,N$. y_j is the teacher data to determine the function $S(\cdot)$. In this regard, the interpolation bases are chosen as $\{\phi(X-X_1), \phi(X-X_2), \dots, \phi(X-X_N)\}$, where $X_1, X_2, \dots, X_N$ are predefined interpolation nodes. With these assumptions, the basis functions are defined as Eq. (1):

$$\phi(r_j) \equiv \phi(\|X-X_j\|) = \sqrt{\|X-X_j\|_2^2+\tau^2}. \tag{1}$$

where $r = \|X\|_2$, $\|\cdot\|_2$ is the Euclidean norm and τ is a shape parameter. The functions are known as RBFs since they depend on the radius. Some of these RBFs are listed in Table 1.

To proceed with 2D interpolation using RBFs $\phi(r)$, we select a linear combination of these functions at the interpolation nodes as follows:

$$S(\mathbf{X}) = \sum_{j=1}^{N} \beta_j \phi(\|\mathbf{X}-\mathbf{X}_j^c\|_2, \tau), \tag{2}$$

where $\mathbf{X} = (x_1, x_2, \dots, x_d)$, τ indicates the shape parameter, β_j is the interpolation coefficient, and $r = \|\mathbf{X}\|_2$. Suppose we want to approximate a function such as $f : \mathbb{R}^d \to \mathbb{R}$ with the proposed interpolator in Eq. (2). To obtain the β_j coefficients, we apply the following interpolation condition:

$$S(\mathbf{X}_i) = f(\mathbf{X}_i), \ i = 1,2,\dots,N \tag{3}$$

Utilizing Eq. (3) at the central points X_j^c for $j = 1,2,\dots,N$, we obtain the following linear system:

$$A\beta = f \tag{4}$$

The above system can be expanded as follows:

$$\underbrace{\begin{bmatrix} \phi(r_{1,1}) & \phi(r_{1,2}) & \dots & \phi(r_{1,N}) \\ \phi(r_{2,1}) & \phi(r_{2,2}) & \dots & \phi(r_{2,N}) \\ \vdots & \vdots & \ddots & \vdots \\ \phi(r_{N-1,1}) & \phi(r_{N-1,2}) & \dots & \phi(r_{N-1,N}) \\ \phi(r_{N,1}) & \phi(r_{N,2}) & \dots & \phi(r_{N,N}) \end{bmatrix}}_{A} \underbrace{\begin{bmatrix} \beta_1 \\ \beta_2 \\ \vdots \\ \vdots \\ \beta_N \end{bmatrix}}_{\beta} = \underbrace{\begin{bmatrix} f(X_1) \\ f(X_2) \\ \vdots \\ \vdots \\ f(X_N) \end{bmatrix}}_{f}, \tag{5}$$

where $r_{i,j} = \|\mathbf{X}_i^c - \mathbf{X}_j^c\|$. The solution of the above system depends on the inverse of the matrix of coefficients A, which is discussed in the next section.

To achieve interpolation, following Eq. (5), we must solve a larger system to approximate the values of f at additional points. It should be emphasized that β is not unknown in the new system of Eq. (7), because it is already derived from system in Eq. (5). The next step is to choose more points from the 2D grid (i.e., $X_j \in [a,b]\times[a,b]$) to create a H matrix with a larger number of rows (depending on the number of approximation points necessary).

The new coefficient matrix is then composed as:

$$H = [h_{ij}]_{M\times N} = [\phi(\|\mathbf{X}_i - \mathbf{X}_j^c\|_2)]_{M\times N}, \ i = 1,2,\dots,M \ , j = 1,2,\dots,N. \tag{6}$$

Finally, the interpolant is evaluated at the M points by the following matrix multiplication:

$$f_{app} = H\beta = HA^{-1}f, \tag{7}$$

where f_{app} indicates the approximated f (i.e., the reconstructed function in our problem).

Remark 1. Higher temporal resolution is achieved by increasing the number of rows of H.

2.2. Invertibility of the interpolation matrix

A necessary and sufficient condition for the well-posing of the interpolation problem is the invertibility of matrix A in Eq. (5). Given that in this paper we use Gaussian and MQ bases, in the following we address the invertibility of the interpolation matrix of these two kinds of functions [29].

Definition 1. The real-value function ϕ on $\mathbb{R}^d$ is positive definite if and only if:

- ϕ be an even function
- for any N distinct points $\mathbf{X}_1, \mathbf{X}_2, \dots, \mathbf{X}_N$ and any vector $c = [c_1, c_2, \dots, c_N]^T$,

$$\sum_{i=1}^{N}\sum_{i=1}^{N} c_i c_j \phi(x_i - x_j) \geq 0 \tag{8}$$

The function ϕ is strictly positive definite if the only vector c that turns the inequality expressed in Eq. (8) into an equality is the null vector.

If ϕ is strictly positive definite, then all of eigenvalues of the interpolation matrix A are positive (hence A is positive definite) and therefore A is invertible.

Theorem 1. *A function ϕ is completely monotone on $[0,\infty)$ if [30]:*

- $\phi \in C[0,\infty)$
- $\phi \in C^{\infty}(0,\infty)$
- $(-1)^l \phi^{(l)}(r) \geq 0$ *where* $r > 0$ *and* $l = 0,1,\dots$

Theorem 2. *If function ϕ is completely monotone on $[0,\infty)$, but not constant, then $\phi(\|\cdot\|^2)$ is strictly positive definite and radial basis on $\mathbb{R}^d$ for all d [30].*

Remark 2. According to Theorems 1 and 2, the Gaussian function is strictly positive and therefore its interpolation matrix is invertible. Also, a simplified version of the Micchelli theorem [31], that guarantees the invertibility of the MQ interpolation matrix, can be found in [29].

Remark 3. Although the matrix A is invertible, the problem remains ill-posed due to the matrix's large condition number. Therefore, in order to control the error we must choose the optimal shape parameter. There are several methods for selecting the shape parameter τ, including the Hardy method in [32] and the Frank method in [33]. In most of the literature, the shape parameter is randomly selected based on the condition number of the interpolation matrix.

2.3. Error analysis

For sufficiently smooth functions, the RBF method has exponential accuracy. For example, the MQ method has a degree of convergence $O(\mathfrak{F}^N)$, where $0 < \mathfrak{F} < 1$, while many other methods, such as the finite differences method, finite element interpolation and polynomial splines, have a degree of convergence $O(N^{-m})$ for a constant m.

For a constant value of the shape parameter (τ), the MQ method is exponentially convergent to the sufficiently smoothed functions. In such a way h, the least upper bound of the distance between X and X_j (i.e., $h = \sup_{X\in\Gamma}(\min_{X_j^c\in\Xi}\|X - X_j^\tau\|)$), is sufficiently reduced. Where Γ is the set of centers and Ξ is the interpolation domain. In this case, the interpolation error can be expressed as:

$$|f(X) - S(X)| \le e^{\frac{-K\tau}{h}}. \tag{9}$$

Elsewhere (in the middle points), the error is given by:

$$|f(X) - S(X)| \le K\mathfrak{F}^{\frac{1}{\tau h}}. \tag{10}$$

Similar results are given for the Gaussian RBFs in [34].

2.4. The proposed structure for increasing temporal resolution using 2D (spatio-temporal) interpolation

In this subsection, it is assumed that an echocardiography video has been converted into a set of frames. Then, w.r.t up-sampling (UpS) rate, we consider certain middle frames with unknown values. The whole image rows' IVTSs are extracted in the following phase, and they are then subjected to the proposed 2D interpolation (see Fig. 1). The rationale behind this idea is that, in addition to the temporal information, incorporation of the spatial information in the interpolation process could be helpful for more accurate reconstruction. Considering that our method is meshless, these choices can be with equal distance or randomly. To increase the temporal resolution, the UpS process should then be used on the selected sample frames. In other words, the UpS process aims at increasing the number of frames using interpolation, which is the main application of the proposed technique for improving frame rate.

In the following, we formalize how 2D technique to the echocardiography frames. Suppose that we need to utilize $S(\cdot)$ to interpolate a function f at interpolation points X_j, such that $f(X_j) = S(X_j)$. Similar to the 1D interpolation case, where a 1D vector (i.e., $X_j \in \mathbf{R}$) is necessary, for 2D interpolation we need a set of points on a 2D grid (i.e., $X_j \in \mathbf{R}^2$). Since we intended to incorporate both spatial and temporal information for reconstruction, 2D interpolation was essential in our suggested technique. So we assumed that $X_j \in [a,b]\times[a,b]$ (specifically, we assumed that $X_j \in [0,1]\times[0,1]$). In the presented strategy, we treat a subset of the frames as known samples. The IVTSs are then calculated using these samples and the interpolation factor. Each point on the IVTS corresponds to a point on the 2D grid ($[a,b]\times[a,b]$). In the proposed approach, we indicate the value of each pixel as $y_j \in R$. The key idea here is to develop an interpolation function, such as $S(\cdot)$, that maps the $\mathbf{R}^2$ space to the $\mathbf{R}$ space. For this purpose, we utilize RBFs defined by the norm because they have the property of mapping from a n-dimensional to a 1D space. As a result, we can easily reduce the problem from higher dimensions to 1D using the RBF technique, hence demonstrating the suggested technique's applicability also to 3D echocardiography. Finally, the values between the frames can be obtained (i.e., by interpolating the values between frames we can increase the temporal resolution as needed.). In similar methods, such as the one from [26], two pixels at the (i,j)th position on the $(k-1)$th and $(k+1)$th frames are used to reconstruct the corresponding pixel in the (i,j)th position on the kth frame. Due to the fact that the location of a given pixel in consecutive frames is constantly changing, especially in areas of the image that present faster movements (for example, the heart valve), the method proposed in [26] creates a significant error. In our proposed method, this problem has been solved using a concept named 2D scattered data interpolation. In other words, the proposed 2D interpolation decreases the reconstruction error by extending the IVTC concept to IVTS through this study while maintaining the beneficial characteristics of the earlier IVTC-based methods.

In general, increasing the frame rate using the proposed 2D RBF interpolation method consists of the five steps listed below:

Step 1 Determining the UpS rate for increasing the frame rate.

Step 2 Creating three-dimensional matrices based on the UpS rate: D for known values based on sample frames and B for unknown values (NaN).

Step 3 Ensuring the well-posing of the two-dimensional interpolation problem by changing the value of the shape parameter (τ) according to the condition number of coefficient matrix (A).

Step 4 Interpolation by solving system Eq. (5) and then determining the unknown values of matrix B using the following close form of solution:

$$S(\mathbf{X}) = \sum_{j=1}^{N} \beta_j \phi(\|\mathbf{X} - \mathbf{X}_j^c\|_2, \tau). \tag{11}$$

Step 5 Extraction of reconstructed IVTSs from 2D RBF interpolation and consequently increasing the temporal resolution of echocardiography images.

In Algorithm 1, we present the steps needed to perform 2D RBF interpolation using the proposed IVTS-based technique. The algorithm needs as input the sample frames as well as the shape parameter value τ. The shape parameter's value is chosen at random. However, in order to achieve the best value, we controlled the shape parameter by examining the coefficients' matrix condition number values. The matrix A is the above mentioned interpolation matrix, which consists of the bases of the approximation space. The matrix H is formed to evaluate the interpolant at arbitrary selected points. In this algorithm, $D_{M\times N_c\times K}$ and $B_{M\times N_c\times Z}$ are 3D structures containing all IVTSs corresponding to the original and the high frame rate video (resulting from the proposed technique), respectively. M is the number of image rows, N_c is the number of image columns, K is the number of frames in the original video, and Z is the number of frames through the high frame rate video (i.e., $Z = UpS \times K$).

Algorithm 1: Applying the proposed 2D RBF interpolation method for enhancing temporal resolution.

Input : $D_{M\times N_c\times K}$, m , τ
/* M : The number of image rows N_c : The number of image columns */
Output: $B_{M\times N_c\times Z}$
1 *Generating* A, H *and* X^c
2 **if** $cond(A) < 10^{+m}$ **then**
  /* Well-posed problem */
3 **for** $i = 1;\ i = M;\ i++$ **do**
4 $F \leftarrow IVTS^i$
5 $\beta \leftarrow A \backslash F$;
6 $f_{App} \leftarrow H * \beta$;
7 $IVTS^i_{new} \leftarrow f_{App}$
8 $B(i,j,:) \leftarrow IVTS^i_{new}$
9 **end**
10 **else**
  /* Ill-posed problem */
11 Change the τ;
12 **end**

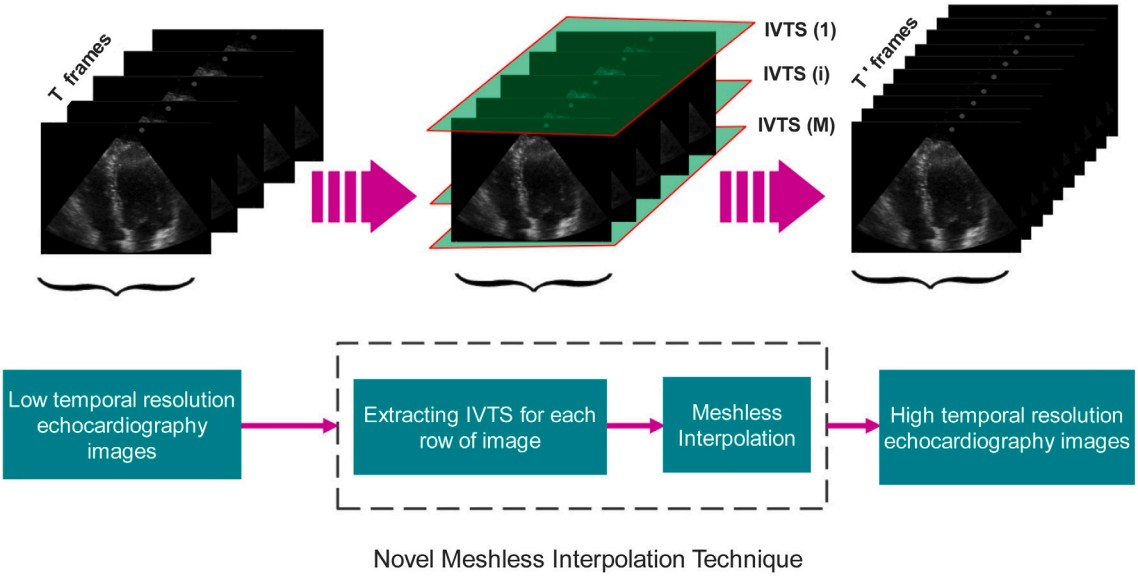

Fig. 1. Block diagram of the proposed approach for increasing the frame rate.

2.5. Data description

In order to demonstrate the efficacy of the suggested strategy in improving the temporal resolution, the proposed method is applied to the following 2D/3D echocardiography datasets:

- **DATASET 1: 2D echocardiography (Bitmap images):** The first dataset includes bitmap echocardiographic frames derived from an ultrasound generated movie of a healthy heart, which consists of 114 frames. A 2MHz probe in combination with a Vivid 3 ultrasound scanner was used to record the data. The frame rate was about 55–68 frames per second and the frame size is 481 by 411 [18]. These frames examine the heart from a four-chambered view.
- **DATASET 2: 2D echocardiography (Real RF data):** Differently from the previous dataset, this dataset consists of data at RF level. Data were acquired by a Verasonics scanner and consist of 50 frames related to a healthy heart. A 64-element probe with a center frequency of 3MHz and 0.3-mm pitch was utilized to do imaging of the heart from the parasternal long-axis view. The sampling frequency was set at four times the center frequency. Each frame is constructed from received ultrasound RF signals generated by 101 focused transmission beams, covering a sector scan from −37.5° to 37.5° [35,36]. The dataset is available online on the UltraSound ToolBox (USTB) website (https://www.ustb.no/ustb-datasets/).
- **DATASET 3: 3D echocardiography (Realistic RF data):** To show the effectiveness of the method in higher dimensions, 3D echocardiography data taken from [37] have also been used. The synthetic probe's characteristics were tuned to closely resemble the transducer's properties used to acquire the template. The ultrasound system, in particular, included a phased array transducer centered at 3.3 MHz and delivering a Gaussian pulse with a −6 dB relative bandwidth of 65%. In addition, the sampling frequency was set at 50 MHz. This dataset includes 34 RF volumes with size 107 × 13637 × 80, where 107 × 80 lines in azimuth and elevation direction were used to create the simulated images, covering an angle of 76° × 76°. The dataset is available online on http://www-sop.inria.fr/asclepios/data/STRAUS/.

2.6. Image quality metrics

Several image quality metrics can be used to assess the reconstruction performance, see [18,38] for details. Generally speaking, these metrics fall into two categories: reference-based metrics, i.e., metrics that compare the obtained images with the original images, and non-reference-based metrics (i.e., metrics that use only the output for evaluation). These metrics are briefly summarized in Table 2.

Table 2
Image quality evaluation criteria.

Name	Abbreviation	Formula
Reference-based		
Mean square error	MSE	$\frac{1}{MN_c}\sum_{i=1}^{M}\sum_{j=1}^{N_c}(I_O - I_R)^2$
Peak signal-to-noise ratio	PSNR	$10 \times \log_{10}(\frac{255}{MSE})$
Structural similarity	SSIM	$\frac{2\mu_R \times \mu_O + C_1}{2\mu_R^2 + \mu_O^2 + C_1} \times \frac{2\sigma_R \times \sigma_O + C_2}{2\sigma_R^2 + \sigma_O^2 + C_2}$
Pratt's figure of merit	FOM	$\left(\max(N_I, N_F)\sum_{i=1}^{N_F}(1+\lambda d_i)^2\right)^{-1}$
Non-reference-based		
Contrast to noise ratio	CNR	$\frac{\lvert\mu_f - \mu_b\rvert}{\sqrt{\sigma_b^2 + \sigma_f^2}}$

Where: $M \times N_c$ is the image size; I_O and I_R are the original and reconstructed images, respectively; μ and σ are the mean and variance of the image intensity values; the constants C_1 and C_2 are used to prevent the denominator of the two fractions in SSIM from becoming zero, usually set to $(0.01 \times 255)^2$ and $(0.03 \times 255)^2$, respectively; μ_f and μ_b are the average intensities in the foreground and background regions; σ_f and σ_b are the standard deviations of these regions; N_I and N_F are the number of ideal and found edge pixels; λ is the penalizing factor for offset edges; and d is the distance between the found edge pixels to the ideal edge pixels.

3. Results and discussion

To evaluate the proposed method, we conduct both qualitative and quantitative analysis. As discussed above, the method has been tested on three clinical echocardiographic datasets, see Section 2.5. The reconstructed frames, related to DATASET 1, are compared to the original frames as well as to the results from [18]. To compare with the original images, the frames are divided into two categories. The known frames used for interpolation fall into the first category (known information), whereas the frames to be compared with the reconstructed frames fall into the second category (unknown information). Examples of these images is shown in Figs. 2(a) and 2(b), where we can see the four-chambered view of the heart as well as the mitral valves.

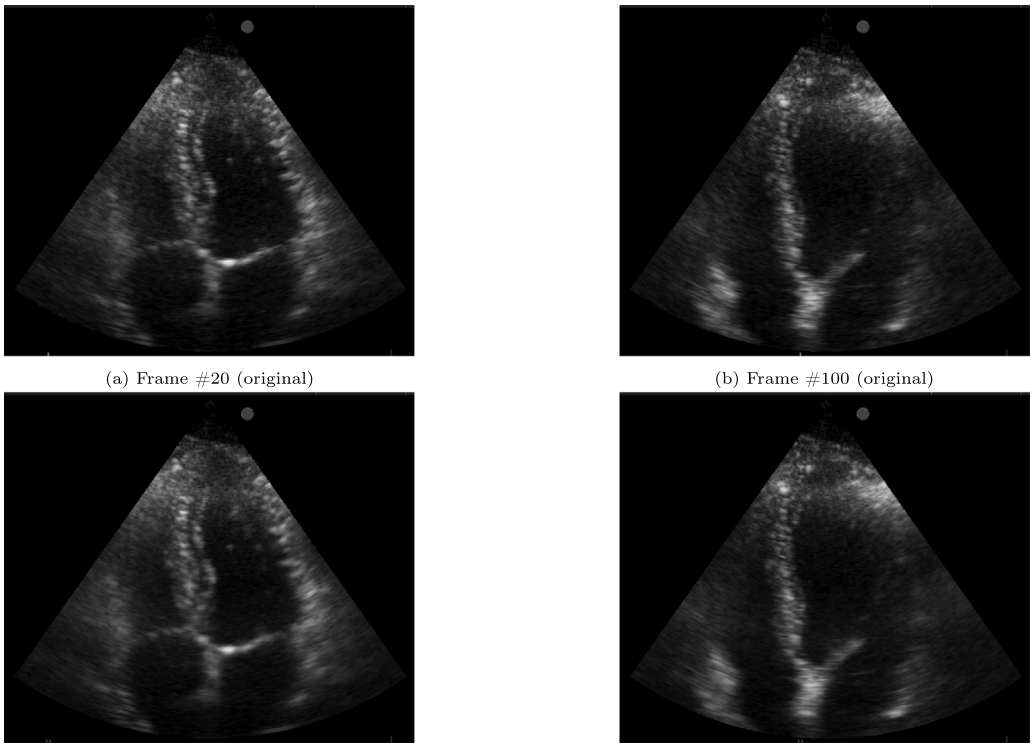

(a) Frame #20 (original) (b) Frame #100 (original)

(c) Frame #20 (Reconstructed) (d) Frame #100 (Reconstructed)

Fig. 2. Two examples of original frames vs. those reconstructed using the proposed technique (for DATASET 1). The first row depicts the original frames, while the second represents the reconstructed frames using the proposed interpolation techniques.

Table 3
Average image quality metrics for reconstructed images with DS rate 2 (for DATASET 1).

Method	MSE	PSNR	SSIM	CNR	FOM
Sparse representation method	0.9039	33.32	0.9834	1.1206	0.8343
B-spline method	0.4382	41.28	**0.9916**	1.6342	0.8795
Radial base function method (Ours)	**0.2424**	**44.36**	0.9707	**2.6272**	**0.9099**

Figs. 3(a) and 3(b) show the original IVTSs of the image row indices of # 170 and # 350, respectively. Moreover, this figure depicts the interpolated IVTSs corresponding to the same rows, as well as its errors for down-sampling (DS) rates of 2 and 3. The figure demonstrates that the suggested interpolation approach reconstructs the original IVTS with an acceptable error, particularly for global information. It should be noted that as the DS rate rises, the resulting IVTS becomes more blurry as a result of a lack of sufficient known information for reconstructing local information (such as the image edges).

The evaluation metrics (MSE, PSNR, SSIM, CNR and FOM) calculated on the reconstructed images are reported in Tables 3 and 4 for DS rates of 2 and 3, respectively. Average value for each metric, across frames, are reported. The results are compared with those obtained by similar methods presented in [18,26]. Generally, our proposed approach shows improved performance. It should be noted that due to the fact that the selected image evaluation criteria are sensitive to different data, our tests are performed on the same data used in [18,26]. An improvement of about 10% PSNR compared indicates that the method is reasonably successful in reducing the image noise. As can be seen in Table 3, the proposed method performs better in all criteria, except for SSIM, where the B-spline method is approximately 2% better. The reason why the proposed method performs better than the existing methods, such as spline and B-spline, is the use of radial base interpolation, in addition to the information in the temporal domain, as well as the spatial information obtained from the neighborhood of each pixel. It is true that simultaneous interpolation has better results in both spatial and temporal domains, but it should not be overlooked that in terms of time complexity we face a larger problem. Quantitatively, the average MSE for the proposed method is 80% and 316% better than that achieved with the B-spline method and the sparse representation method, respectively. The RBF method also performs better in reconstructing the edges of images. This can be easily understood by comparing the FOM values in Table 3. Our method also performs better with respect to the other metrics, such as CNR. Overall, RBFs are a good alternative to polynomial-based methods. In the Supplementary Material We provide the original and reconstructed videos as supplementary material, available at,[2] the file named `d1-original.avi` contains an original echocardiographic clip with a frame size of 411 × 481, which is recorded at a rate of 45 frames per second. The file named as `RBF.echo.ds2.avi` is a reconstructed video obtained by means of radial basis interpolation at the same frame rate. Also, the two files named as `RBF.echo.ds3.avi` and `RBF.echo.ds5.avi` are obtained by the proposed method with DS set to 3 and 5, respectively. To view the reconstructed videos at a higher frame rate, we performed UpS on the original frames by using the proposed method. Two examples of reconstructed videos with UpS at 40 and 80 frames per second can be seen in files `RBF.echo.us2fr40.avi` and `RBF.echo.us2fr80.avi`, respectively.

In addition, we summarized the boxplots of MSE, SSIM, and FOM in Figs. 4, 5, and 6, respectively. The variations are specified over all the frames for different DS rates. Fig. 4 shows that we can increase the frame rate by 5 times while the MSE is still less than 0.42. Also, as it can be seen from Fig. 5, the SSIM values are larger than 90% for DS rates of 2, 3, and 4. However, when applying the proposed approach, the SSIM ranges from 85% to 92% for all the frames. Therefore, the results of this

[2] https://drive.google.com/file/d/1svHmJVyv4pfCuka9dr4YwDNvt-E0TPfn/view?usp=sharing.

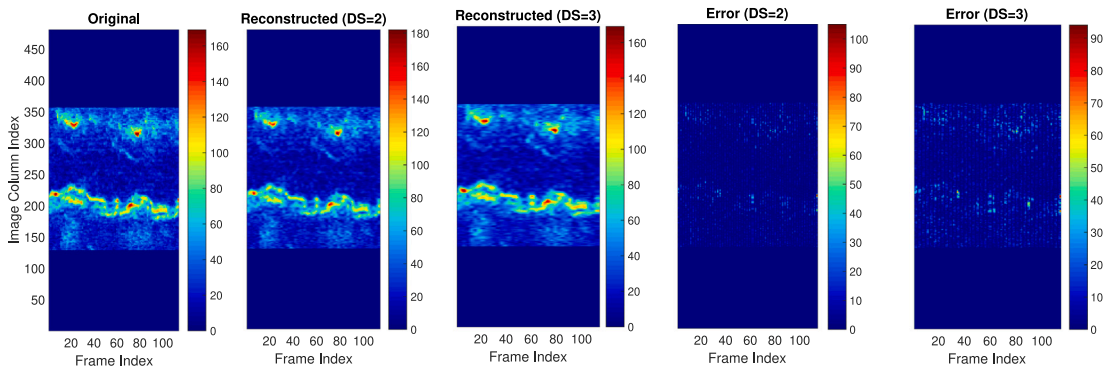

(a) Image row index #170

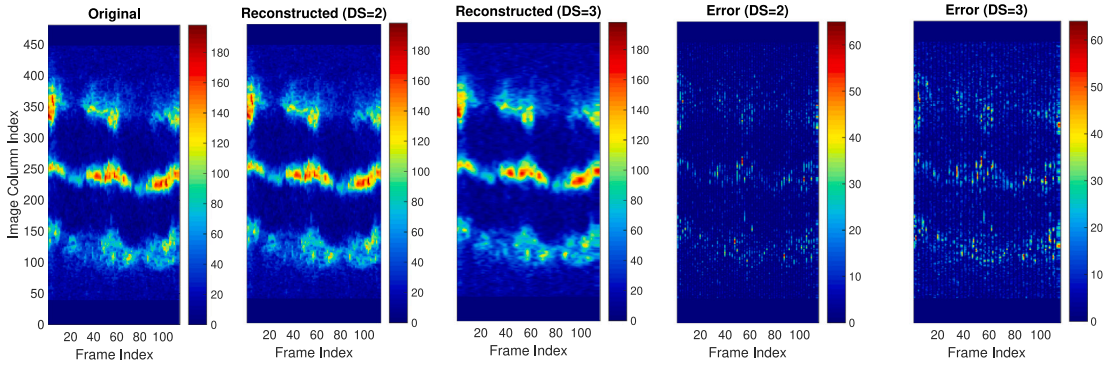

(b) Image row index #350

Fig. 3. The heat-maps of the original IVTS (for DATASET 1), the reconstructed IVTS, and their error achieved by the proposed 2D interpolation with DS rates of 2 and 3. (The results are shown for image row indices of (a) # 170 and (b) # 350). The color bars depict various IVTS pixel intensity values. Warmer colors denote higher intensity values of the IVTSs, whereas colder colors denote lower intensity values.

Table 4
Average image quality metrics for reconstructed images with DS rate 3 (for DATASET 1).

Method	MSE	PSNR	SSIM	CNR	FOM
Sparse representation method	0.9228	33.13	0.9253	1.0040	0.7812
B-spline method	0.6721	40.65	**0.9637**	1.1514	0.8123
Radial base function method	**0.3861**	**43.91**	0.9544	**2.1510**	**0.8991**

Table 5
Processing time (second) for reconstructing by DS rate 2 (for DATASET 1).

	Sparse representation	B-spline	RBF (proposed)
Time to run (s)	11 253	59	55

analysis show that we can increase the frame rate of echocardiography by 4 times while the SSIM is larger than 90%. Finally, we should analyze the increasing frame rate based on the FOM metric. This metric is often used to evaluate the power of a reconstruction algorithm in terms of image details recovery (such as for the edges), so that for perfect reconstruction the FOM would be 1. Fig. 6 shows the boxplot for FOM and as it can be seen from the figure, this value is larger than 85%, which indicates that we can increase the frame rate by 5 times while the edge information recovery quantified by FOM is larger than 85%. However, we have a trade-off between the frame rate and the performance in terms of FOM. In other words, when the details of images are very important, it is better to have a FOM larger than 90%; this implies that we can increase the frame rate up to 4 times.

One concern with the interpolation techniques is their computational complexities, which should also be addressed in this study. Assume that the matrix $A_{N\times N}$ is an interpolation matrix for a system of radial base functions, in which case the inversion and multiplication of A has $O(N^3)$ complexity. Now, if we want to reconstruct IVTS from 1 to M (M: the number of image rows) to increase the time resolution in an ultrasound video, the overall time complexity of the method is $O(M \times N^3)$. In our problem, N (i.e., the dimension of interpolator matrix in Eq. (4)) is a fraction of the total number of frames by the DS factor ($N = \frac{K}{DS}$). This shows that the complexity of the interpolation in this case, which is due to the inversion of the interpolator matrix, is increased when employing lower DS rates (i.e., higher dimension of A). Table 5 shows the time required to execute the image reconstruction process using three methods: B-spline, sparse representation method and the proposed RBF method. All methods are run on a 64-bit system with Intel® CoreTM i7–8700 K CPU @ 3.70 GHz and 32 GB RAM. As can be seen in Table 5, the proposed method is the fastest, while the sparse representation method is significantly slower. It should also be noted that the proposed method requires 29 and 19 s to reconstruct the images using DS rates of 3 and 5, respectively. Regarding the explanation for this, it should be emphasized that the computational complexity depends on the dimension of the known information, or interpolator A in Eq. (4).

Another investigation that is crucial in this study is the parameter setting. The only parameter that must be set in the proposed 2D interpolation technique is the shape parameter (τ). As a consequence, an analysis is required to investigate the sensitivity of the reconstruction error to this parameter. To accomplish this, we ran the reconstruction while changing this parameter. Finally, we calculated the MSE corresponding to each value of this parameter. The results are summarized in Fig. 7 for different DS rates. As we expected, as the DS rate rises, the reconstruction error also rises because there is less information available at higher DS rates. On the other hand, the trend shows that

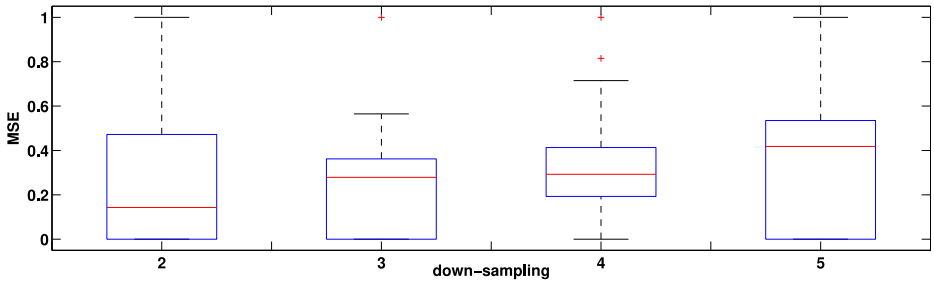

Fig. 4. MSE boxplot for different DS rates with the proposed RBF method (for DATASET 1).

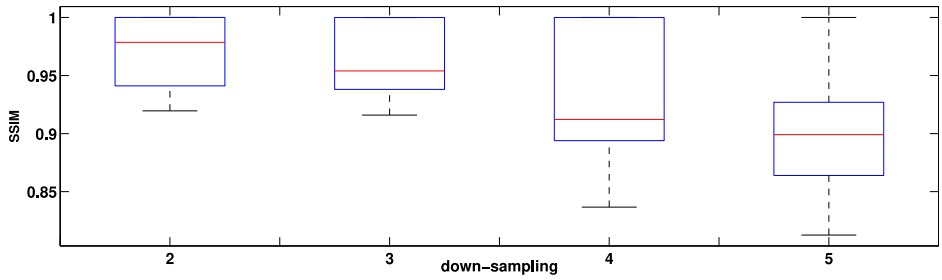

Fig. 5. SSIM boxplot for different DS rates with the proposed RBF method (for DATASET 1).

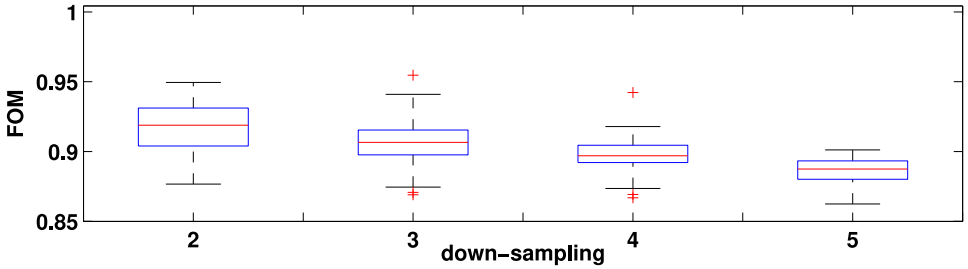

Fig. 6. FOM boxplot for different DS rates with the proposed RBF method (for DATASET 1).

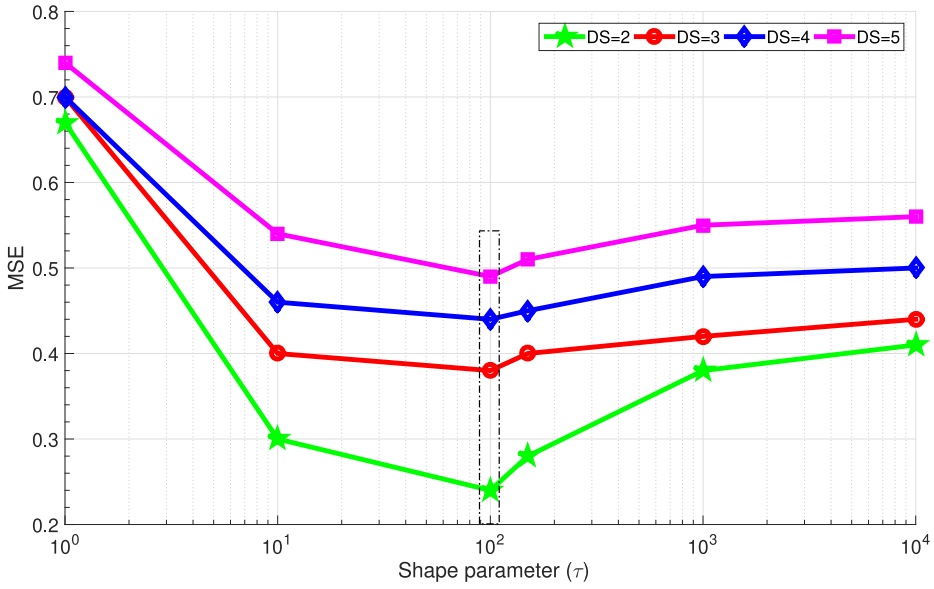

Fig. 7. Sensitivity of the reconstruction error (i.e., MSE) to the shape parameter τ (for DATASET 1). The dash lines specifies the ranges of the shape parameter leads to the best reconstruction performance.

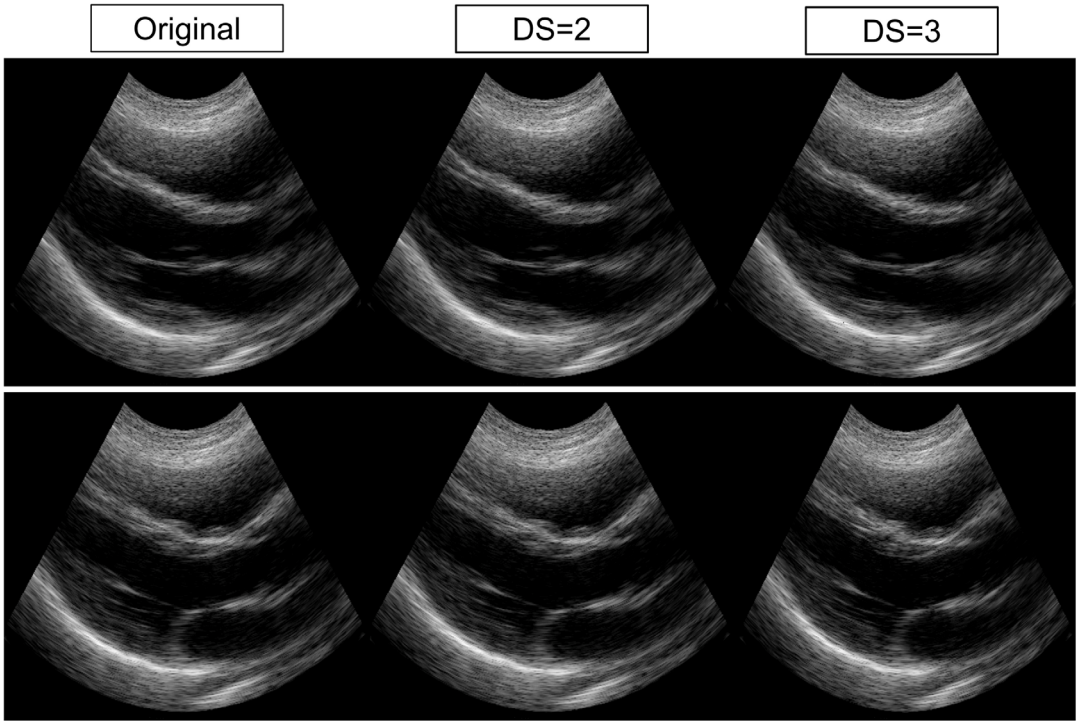

Fig. 8. Two examples of original frames vs. those reconstructed using the proposed technique (related to DATASET 2). The first column depicts the original frames, while the second and third ones represent the reconstructed frames using the proposed interpolation technique. Frame #20 and #30 are shown in the first and second rows, respectively (see the link to the original and reconstructed videos).

Table 6
Average image quality metrics for 2D reconstructed images with RBF interpolation (for DATASET 2).

	Original	Ours (DS = 2)	Ours (DS = 3)	Ours (DS = 4)
MSE	–	0.3298	0.4755	0.5812
SSIM	1.0000	0.9818	0.9738	0.9675
PSNR	–	69.84	60.13	55.12
FOM	1.0000	0.9326	0.9006	0.8935

the MSE value monotonically decreases while the τ value increases from 1 to 100. However, for $\tau > 100$, the MSE rises as τ increases, and the trend reaches saturation for $\tau > 1000$. In addition, the findings of the figure demonstrate that best value of this parameter to reach the minimum MSE is around $\tau = 100$ (i.e., $m = 2$). All the results reported in this paper were obtained setting the shape parameter as $\tau = 100$.

Additionally, we applied the proposed reconstruction technique to the 2D RF level echocardiography database (DATASET 2). We utilized the delay and sum (DAS) beamformer to construct the frames. Finally, considering different DS/UpS Rate, the proposed technique was applied to get the missing/additional information. Two examples of the results for different DS rates are shown in Fig. 8. Moreover, we quantified the image quality metrics for both the original and reconstructed video frames (see Table 6). The qualitative and quantitative results indicate good image quality metrics ($SSIM \geq 93\%$), demonstrating the strength of the suggested technique in the estimation of the missing information. Therefore, the results on the dataset revealed that the applicability of the proposed technique is not limited to the outermost layer of the post-processing (i.e., bitmap frames), but it is also extendable to the beamforming stage, where the technique can be used to add additional middle beamformed frames at RF level considering the known information of the already beamformed data. Applying this technique not only brings us additional useful information, but also significantly saves the computational time (see Table 7).

We carried out another experiment to demonstrate the feasibility of adapting our method to 3D echocardiography, where the requirement for higher frame rates is even more critical. In this regard, we present the results of the suggested approach on the post-beamformed RF data with 34 volume sequences. Specifically, Fig. 9 shows the frame 20 (from different 3 views) of the baseline data and the reconstructed one for DS rates of 2 and 3. Similar to two previous datasets, we compared the image quality metrics of the original and the reconstructed frames (see Table 8). The results demonstrate an acceptable reconstruction error in terms of image quality criteria (e.g., $SSIM \geq 90\%$ for a DS rate of 3, and $SSIM \geq 86\%$ for a DS rate of 4), which allows us to increase the frame rate of 3D echocardiography by 3 to 4 times. It should be noted that the real-world application of the proposed technique is in the upsampling process, where the amount of known data is larger than in the downsampling process. Due to this fact, the suggested technique yields a more accurate estimation for the middle frames (see the link to the baseline and higher frame rate data using different UpS rates). In addition, Table 9 summarizes the reconstruction technique execution time for 3D echocardiography data (DATASET 3) at various DS rates.

Motion estimation is another critical evaluation that must be performed when using reconstruction approaches. In other words, the reconstruction technique should preserve the motion information through the whole video with an acceptable accuracy. In this regard, we utilized the speckle tracking tool for the motion estimation (DATASET 2 was used for this assessment). Specifically, we used the MATLAB Ultrasound Toolbox (MUST) [39] for speckle tracking (see the Link to the speckle tracked video). Next, we calculated the horizontal and vertical motion fields for each frame. Finally, we overlaid the motion displacement (with a frame increment of 1) on the M-mode image. The results are shown in Fig. 10. As the results demonstrate, the proposed technique is successful in the motion estimation for DS = 2.

Finally, it is worthwhile noting that the proposed RBF's positive definite bases impose fewer constraints on its application to various problems. Another benefit of this approach is that, when data become dense, it frequently exhibits fast convergence to the approximated function. When compared to spline methods, this method's meshless property allows for greater freedom in selecting nodal points for interpolation. The smoothness of the bases can be adjusted using the

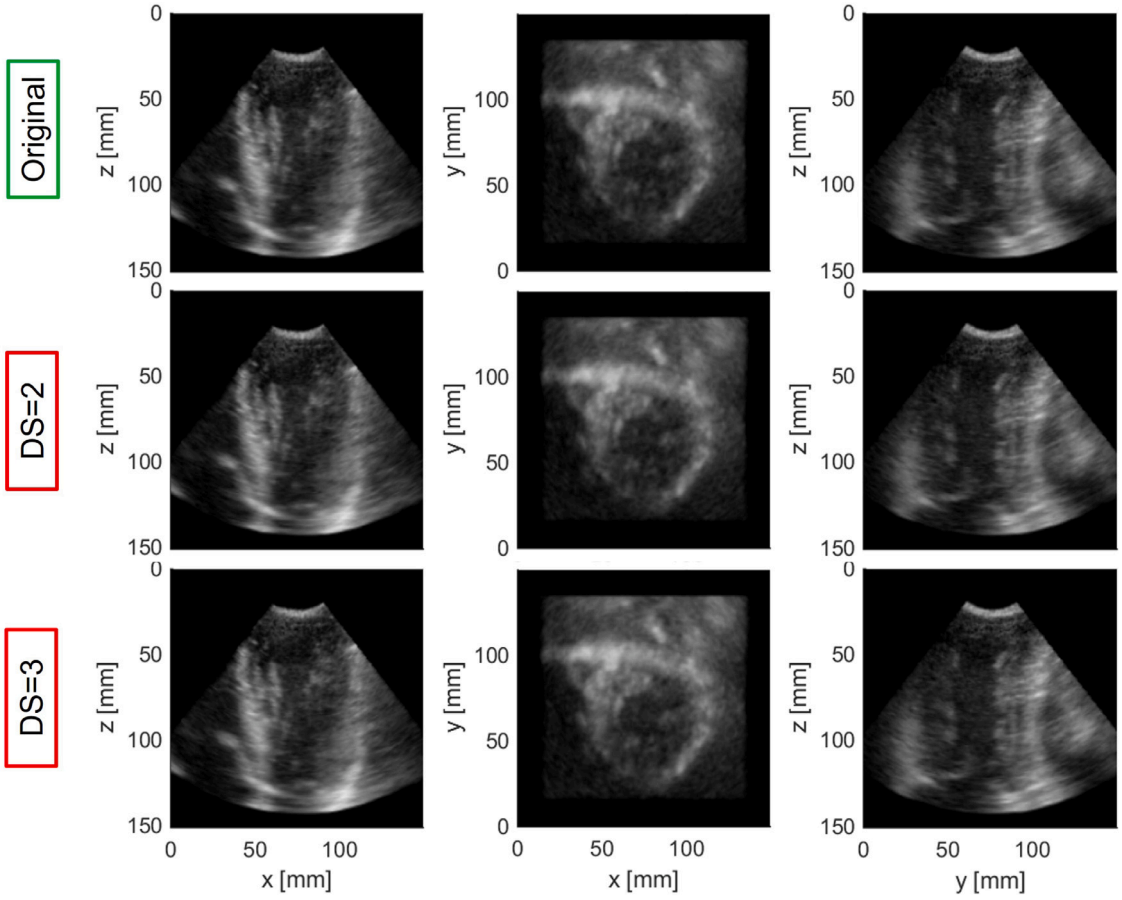

Fig. 9. A 3D echocardiographic frame (Frame#20) reconstructed using our proposed technique at different DS rates (DATASET 3). The first, second, and third columns show this frame from different views in 'x–z', 'x–y', and 'y–z' coordinates, respectively (see the link to the original and reconstructed videos).

Table 7
The beamforming times of echocardiography frames (DATASET 2) when using DAS beamforming and the proposed reconstruction technique.

	Original	DS = 2	DS = 3	DS = 4
Run time	144.47	88.30 s	61.05 s	46.11 s

shape parameter of the RBF method. Both the noise and the error resulting from the approximation can be decreased by optimizing the shape parameter. The proposed method is effective, straightforward, and computationally appealing.

As for the main limitations of the proposed technique, we can indicate that, although the coefficient matrix is non-singular, the condition number of the equation system in Eq. (5) is large. Therefore, the existence of little noise in the original images may lead to significant noise in the reconstructed images. To overcome this issue, the condition number of the coefficient matrix must be monitored and adjusted. Also, one should avoid choosing the shape parameters that lead to an increase of the condition number of the coefficient matrix. As another limitation, the determination of the $S(\cdot)$ function in the case of 3D imaging is difficult due to the limited number of known information (i.e., teacher data), which leads to introduce motion artifacts. However, this problem applies not only to our proposed technique, all the reconstruction techniques consider the known data and estimate the missing data accordingly. Therefore, this issue is not related specifically to our reconstruction tool but rather to the limited quantity of data available in 3D scenarios.

Table 8
Average image quality metrics for 3D reconstructed images (DATASET 3) with RBF interpolation.

	Original	Ours (DS = 2)	Ours (DS = 3)	Ours (DS = 4)
MSE	–	0.3417	0.5228	0.6023
SSIM	1.0000	0.9342	0.9018	0.8651
PSNR	–	65.50	52.32	47.81
FOM	1.0000	0.9369	0.8914	0.8379
CNR ('x-z' view)	1.3315	1.3134	1.3108	1.3178
CNR ('x-y' view)	0.5591	0.5583	0.5571	0.5567
CNR ('y-z' view)	1.4312	1.4300	1.4168	1.4293

Table 9
Processing time for reconstructing 3D echocardiography (DATASET 3) with different DS rates using 2D RBF interpolation.

	DS = 2	DS = 3	DS = 4
Run time	293.13 s	228.24 s	189.34 s

4. Conclusion

The present study proposes a methodology to increase the temporal resolution of echocardiographic images based on both spatio-temporal information. The main finding of this paper is the use of a 2D RBF interpolator to receive and reconstruct information simultaneously in the spatial and temporal domains. This interpolation method has exponential convergence speed. Another strength of this method is the use of a 2D signal called IVTS, which by passing through all the sample

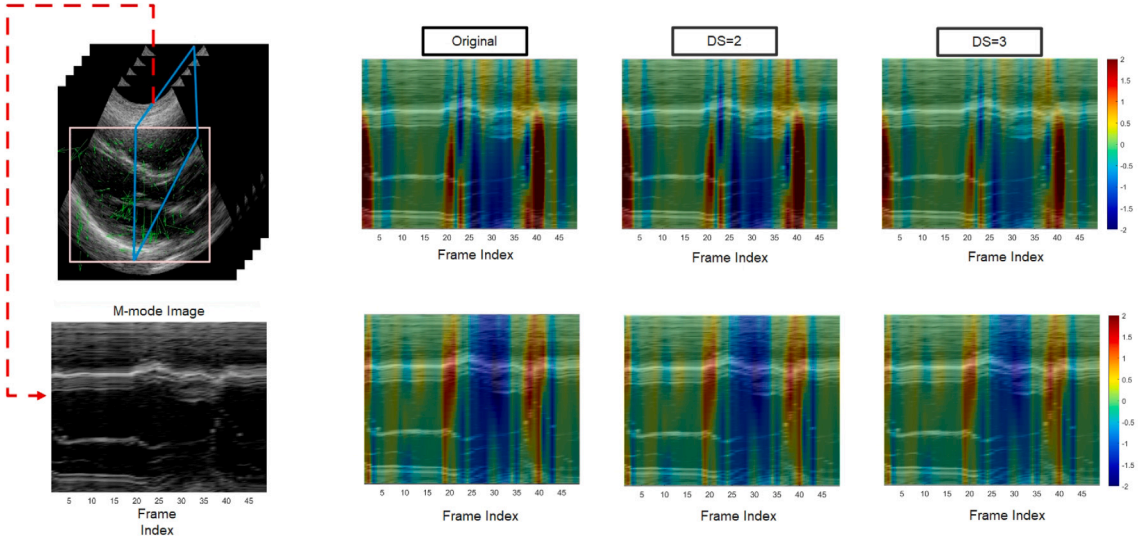

Fig. 10. Motion displacement overlaid to the corresponding M-mode image ('unit = pixel per frame') for DATASET 2. The first and second rows show the horizontal and vertical displacement for the whole video. The second dataset has been used for this evaluation.

frames and receiving spatial and temporal information, allows the 2D interpolation of echocardiography data. To increase the frame rate with the help of this method, we need to increase the number of points on the IVTSs with the help of 2D RBF interpolation. Because there is no mesh in this method, it is possible to increase the resolution in any desired part of the echocardiography videos. Another significant feature of the suggested approach is the inclusion of a shape parameter to regulate the smoothness of the interpolation bases and improve the performance of the reconstruction. This would be beneficial, particularly when trying to estimate local information like speckle noise and image edges. According to the study's findings, the proposed method performs more effectively in terms of speed and accuracy compared to more traditional interpolation techniques. The proposed approach performs significantly better than existing approaches like B-spline and sparse representation by lowering the number of samples required for interpolation. This can be attributed to the sharing of spatial and temporal information for more accurate interpolation, which was only made possible with the aid of the 2D interpolation.

Since the RBF method has a high ability for high-dimensional interpolation, as a suggested example for future work, we can mention the increase in resolution in echocardiographic images using 3D interpolation. Furthermore, the combination of the proposed interpolation method with some acquisition modalities (e.g., plane wave imaging [40,41] or synthetic transmit aperture [42]) is recommended to further increase the frame rate and the data acquisition rate.

CRediT authorship contribution statement

Hamed Jalilian: Methodology, Software, Validation, Visualization, Writing – original draft, Writing – review & editing. **Sajjad Afrakhteh:** Conceptualization, Data curation, Formal analysis, Investigation, Methodology, Software, Validation, Visualization, Writing – original draft, Writing – review & editing. **Giovanni Iacca:** Conceptualization, Investigation, Methodology, Project administration, Supervision, Validation, Writing – review & editing. **Libertario Demi:** Conceptualization, Investigation, Methodology, Project administration, Supervision, Validation, Writing – review & editing.

Declaration of competing interest

The authors declare that they have no known competing financial interests or personal relationships that could have appeared to influence the work reported in this paper.

Data availability

Data will be made available on request.

Acknowledgment

We would like to acknowledge and give warm thanks of Dr. Hamid Behnam for making his clinical data (DATASET 1) available for this research.

References

[1] T. Szabo, Diagnostic Ultrasound Imaging: Inside Out, Academic Press, 2004.
[2] C.M.A. Botelho, J.L.B. Pena, B.R. Passos, P.R.L. Fortes, M.d.C.V. Moreira, Chronic obstructive pulmonary disease: The role of myocardial deformation indices and right ventricle three-dimensional echocardiography, Int. J. Cardiovasc. Sci. 35 (2022) 329–339.
[3] Y. Ma, R.J. Housden, A. Fazili, A.V. Arujuna, K.S. Rhode, Real-time registration of 3D echo to x-ray fluoroscopy based on cascading classifiers and image registration, Phys. Med. Biol. 66 (5) (2021) 055019.
[4] S. Afrakhteh, G. Iacca, L. Demi, High frame rate ultrasound imaging by means of tensor completion: Application to echocardiography, IEEE Trans. Ultrason. Ferroelectr. Freq. Control 70 (1) (2022) 41–51.
[5] D.P. Shattuck, M.D. Weinshenker, S.W. Smith, O.T. von Ramm, Explososcan: A parallel processing technique for high speed ultrasound imaging with linear phased arrays, J. Acoust. Soc. Am. 75 (4) (1984) 1273–1282.
[6] F. Prieur, B. Dénarié, A. Austeng, H. Torp, Correspondence-Multi-line transmission in medical imaging using the second-harmonic signal, IEEE Trans. Ultrason. Ferroelectr. Freq. Control 60 (12) (2013) 2682–2692.
[7] L. Demi, A. Ramalli, E. Boni, J. D'hooge, Orthogonal frequency division multiplexing combined with multi line transmission for ultrafast ultrasound imaging: Experimental findings, in: 2018 IEEE International Ultrasonics Symposium, IUS, IEEE, 2018, pp. 1–4.
[8] G. Zurakhov, L. Tong, A. Ramalli, P. Tortoli, J. D'hooge, Z. Friedman, D. Adam, Multiline transmit beamforming combined with adaptive apodization, IEEE Trans. Ultrason. Ferroelectr. Freq. Control 65 (4) (2018) 535–545.
[9] L. Demi, J. Viti, L. Kusters, F. Guidi, P. Tortoli, M. Mischi, Implementation of parallel transmit beamforming using orthogonal frequency division multiplexing-achievable resolution and interbeam interference, IEEE Trans. Ultrason. Ferroelectr. Freq. Control 60 (11) (2013) 2310–2320.
[10] S. Afrakhteh, H. Behnam, A fast and high frame rate adaptive beamforming using DCT-based RF-line recovery in line-by-line ultrasound imaging, Int. J. Imaging Syst. Technol. 30 (4) (2020) 1080–1094.
[11] S. Wang, W.-N. Lee, J. Provost, J. Luo, E.E. Konofagou, A composite high-frame-rate system for clinical cardiovascular imaging, IEEE Trans. Ultrason. Ferroelectr. Freq. Control 55 (10) (2008) 2221–2233.
[12] J. Provost, W.-N. Lee, K. Fujikura, E.E. Konofagou, Electromechanical wave imaging of normal and ischemic hearts in vivo, IEEE Trans. Med. Imaging 29 (3) (2009) 625–635.

[13] D.P. Perrin, N.V. Vasilyev, G.R. Marx, P.J. del Nido, Temporal enhancement of 3D echocardiography by frame reordering, JACC: Cardiovasc. Imaging 5 (3) (2012) 300–304.
[14] P. Gifani, H. Behnam, Z.A. Sani, A new method for pseudo-increasing frame rates of echocardiography images using manifold learning, J. Med. Signals Sens. 1 (2) (2011) 107.
[15] T. Thaipanich, P. Wu, C.C. Kuo, Robust video frame rate up-conversion (FRUC) techniques, in: Consumer Electronics, ICCE'09. Digest of Technical Papers International Conference, Vol. 3, 2009, pp. 1–2, http://dx.doi.org/10.1109/ICCE.2009.5012254.
[16] W. Zhang, et al., Spatio-temporal (2D+ T) non-rigid registration of real-time 3D echocardiography and cardiovascular MR image sequences, Phys. Med. Biol. 56 (5) (2011) 1341, http://dx.doi.org/10.1088/0031-9155/56/5/008.
[17] X. Huang, et al., Dynamic 3D ultrasound and MR image registration of the beating heart, Med. Image Comput. Comput.-Assist. Interv.–MICCAI 8 (2) (2005) 171–178, http://dx.doi.org/10.1007/11566489_22.
[18] P. Gifani, H. Behnam, F. Haddadi, Z.A. Sani, M. Shojaeifard, Temporal super resolution enhancement of echocardiographic images based on sparse representation, IEEE Trans. Ultrason. Ferroelectr. Freq. Control 63 (1) (2015) 6–19.
[19] M. Hosseinpour, H. Behnam, M. Shojaeifard, Temporal super resolution of ultrasound images using compressive sensing, Biomed. Signal Process. Control 52 (2019) 53–68.
[20] J. Yu, L. Lavery, K. Kim, Super-resolution ultrasound imaging method for microvasculature in vivo with a high temporal accuracy, Sci. Rep. 8 (1) (2018) 1–11.
[21] H.N. Mirarkolaei, S.R. Snare, A.H.S. Solberg, A robust bidirectional motion-compensated interpolation algorithm to enhance temporal resolution of 3D echocardiography, Biomed. Signal Process. Control 65 (2021) 102384.
[22] S. Khoubani, M.H. Moradi, A fast quaternion wavelet-based motion compensated frame rate up-conversion with fuzzy smoothing: application to echocardiography temporal enhancement, Multimedia Tools Appl. 80 (6) (2021) 8999–9025.
[23] D. Liu, Z. Wang, Y. Fan, X. Liu, Z. Wang, S. Chang, X. Wang, T.S. Huang, Learning temporal dynamics for video super-resolution: A deep learning approach, IEEE Trans. Image Process. 27 (7) (2018) 3432–3445.
[24] C. Szegedy, W. Liu, Y. Jia, P. Sermanet, S. Reed, D. Anguelov, D. Erhan, V. Vanhoucke, A. Rabinovich, Going deeper with convolutions, in: Proceedings of the IEEE Conference on Computer Vision and Pattern Recognition, 2015, pp. 1–9.
[25] F. Taheri Dezaki, H. Girgis, R. Rohling, K. Gin, P. Abolmaesumi, T. Tsang, Frame rate up-conversion in echocardiography using a conditioned variational autoencoder and generative adversarial model, in: International Conference on Medical Image Computing and Computer-Assisted Intervention, Springer, 2019, pp. 705–713.
[26] M. Jalali, et al., Temporal super-resolution of 2D/3D echocardiography using cubic B-spline interpolation, Biomed. Signal Process. Control 58 (2020) 101868, http://dx.doi.org/10.1016/j.bspc.2020.101868.
[27] S. Afrakhteh, H. Jalilian, G. Iacca, L. Demi, Temporal super-resolution of echocardiography using a novel high-precision non-polynomial interpolation, Biomed. Signal Process. Control 78 (2022) 104003.
[28] S. Afrakhteh, H. Jalilian, G. Iacca, L. Demi, Increasing the frame rate of echocardiography images based on a novel interpolation technique, in: 2022 IEEE International Ultrasonics Symposium, IUS, IEEE, 2022, pp. 1–4.
[29] A.S. Scott, E.J. Kansa, Multiquadric radial basis function approximation methods for the numerical solution of partial differential equations, Adv. Comput. Mech. 2 (1—220) (2009).
[30] P. Assari, H. Adibi, M. Dehghan, A numerical method for solving linear integral equations of the second kind on the non-rectangular domains based on the meshless method, Appl. Math. Model. 37 (2013) 9269–9294, http://dx.doi.org/10.1016/j.apm.2013.04.047.
[31] C. Micchelli, Interpolation of scattered data: Distance matrices and conditionally positive definite functions, Constr. Approx. 2 (1986) 11–22.
[32] R. Hardy, Multiquadric equations of topography and other irregular surfaces, J. Geophys. Res. 176 (1971) 1905—1915.
[33] R. Franke, Scattered data interpolation: test of some methods, Math. Comp. 38 (1982) 181–200.
[34] H. Wendland, Scattered Data Approximation, Cambridge University Press, 2005.
[35] O.M.H. Rindal, S. Aakhus, S. Holm, A. Austeng, Hypothesis of improved visualization of microstructures in the interventricular septum with ultrasound and adaptive beamforming, Ultrasound Med. Biol. 43 (10) (2017) 2494–2499.
[36] A. Rodriguez-Molares, O.M.H. Rindal, O. Bernard, A. Nair, M.A.L. Bell, H. Liebgott, A. Austeng, et al., The ultrasound toolbox, in: 2017 IEEE International Ultrasonics Symposium, IUS, IEEE, 2017, pp. 1–4.
[37] M. Alessandrini, M. De Craene, O. Bernard, S. Giffard-Roisin, P. Allain, I. Waechter-Stehle, J. Weese, E. Saloux, H. Delingette, M. Sermesant, et al., A pipeline for the generation of realistic 3D synthetic echocardiographic sequences: Methodology and open-access database, IEEE Trans. Med. Imaging 34 (7) (2015) 1436–1451.
[38] S. Afrakhteh, H. Behnam, Low-complexity adaptive minimum variance ultrasound beam-former based on diagonalization, Biomed. Signal Process. Control 62 (2020) 102–110, http://dx.doi.org/10.1016/j.bspc.2020.102110.
[39] D. Garcia, Make the most of MUST, an open-source Matlab UltraSound Toolbox, in: 2021 IEEE International Ultrasonics Symposium, IUS, IEEE, 2021, pp. 1–4.
[40] S. Afrakhteh, H. Behnam, Coherent plane wave compounding combined with tensor completion applied for ultrafast imaging, IEEE Trans. Ultrason. Ferroelectr. Freq. Control 68 (10) (2021) 3094–3103.
[41] M. Hashemseresht, S. Afrakhteh, H. Behnam, High-resolution and high-contrast ultrafast ultrasound imaging using coherent plane wave adaptive compounding, Biomed. Signal Process. Control 73 (2022) 103446.
[42] S. Afrakhteh, H. Behnam, Efficient synthetic transmit aperture ultrasound based on tensor completion, Ultrasonics 117 (2021) 106553.